scientific reports

Check for updates

OPEN

The role of HMOX1-mediated ferroptosis in blue light-induced damage to retinal pigment epithelium

Chunyi Ji[1,2,4], Yiqi Wang[1,2,4], Yahan Ju[1,2], Siwei Liu[1,2], Xirui Chen[1,2], Jiajing Wang[3], Na Sun[3], Zhimin Tang[1,2]✉, Ping Gu[1,2]✉ & Jing Ji[1,2]✉

Currently, blue light irradiation is frequently encountered in daily life and is widely considered a high-risk factor for retinal damage. In particular, blue light-induced dysfunction and death of the retinal pigment epithelium (RPE) may ultimately contribute to irreversible vision impairment and even blindness. However, the underlying pathogenic mechanism and pathogenically targeted protection against blue light-induced RPE degeneration remain unclear. In this study, through sophisticated biochemical evaluation and high-throughput sequencing, the predominant pathological process during blue light-induced RPE degeneration was confirmed to be HMOX1-mediated RPE ferroptosis, which may be involved in the Nrf2–SLC7A11–HMOX1 hierarchy. Upon further knockdown of HMOX1 with si-HMOX1 or the HMOX1 inhibitor zinc protoporphyrin (ZnPP), specific inhibition of HMOX1 overexpression significantly suppressed RPE ferroptosis. In mice, treatment with ZnPP effectively rescued RPE degeneration and visual function. These results highlighted that HMOX1-mediated ferroptosis might be a potential target for protection against blue light-induced damage to RPE cells.

Keywords Ferroptosis, Blue light, HMOX1, Retinal pigment epithelium

Blue light is a short-wavelength light that carries great energy in the visible spectrum[1] and has long been considered a high-risk factor for retinal damage. In recent years, with the development of advanced lighting technology, we have been increasingly exposed to artificial light sources, including LED lamps, smartphone screens, and computer monitors[2]. As the main spectral component of these devices, blue light, with a wavelength of 400–500 nm, has been reported to be the most harmful visible light to human eyes[3–5], and removing the blue light component from light exposure could significantly reduce retinal damage[6]. Thus, the visual safety of these electronic devices has become a crucial issue.

Retinal tissue is susceptible to photodamage, and retinal photodamage can lead to degeneration of the retina. In 1996, Noell et al. reported for the first time that light exposure can cause retinal degeneration in rats[7]. A series of subsequent studies have demonstrated that blue light photodamage contributes to the onset and progression of retinal diseases, particularly age-related macular degeneration (AMD), which is a major cause of irreversible vision loss in developed countries[8,9]. Among the elaborate retinal structures, the retinal pigment epithelium (RPE) is a monolayer of regular polygonal cells located between the bruch membrane and the photoreceptor layer[10] and plays a vital role in visual function and homeostasis of the retina[11]. The crucial functions of the RPE include providing nutrition for the outer cells of the retinal neuroepithelial layer[12], phagocytosing photoreceptor outer segments[13], and maintaining retinal metabolism[14]. Thus, adverse stimulation of the RPE, such as with blue light, may cause damage to the retina, which ultimately results in irreversible vision impairment and even blindness[15]. Early studies revealed that blue light exposure, even at a low luminance, can induce RPE injury in vitro and result in fundus damage, retinal thinning, and neuron transduction impairment in vivo[16]. Morphological changes and cell death in blue light-exposed RPE cells and photoreceptors, similar to those in the degenerating retina[17,18], were further observed. Through continuous exploration of the specific pathogenesis of blue light-induced retinal toxicity, inflammation[19], oxidative stress[20,21], apoptosis[22], autophagy[23], and necroptosis[24] have been shown to

[1]Department of Ophthalmology, Shanghai Ninth People's Hospital, Shanghai Jiao Tong University School of Medicine, Shanghai 200011, P.R. China. [2]Shanghai Key Laboratory of Orbital Diseases and Ocular Oncology, Shanghai 200011, P.R. China. [3]Department of Ophthalmology, Shanghai Tenth People's Hospital, School of Medicine, Tongji University, Shanghai 200072, China. [4]Chunyi Ji and Yiqi Wang contributed equally to this work. ✉email: zhimin888@sjtu.edu.cn; guping2009@126.com; flowerrainday@sina.com

be involved. Nevertheless, some degenerative processes still cannot be explained. Therefore, further studies are needed to investigate the exact mechanism of blue light-induced RPE damage.

Ferroptosis, a novel type of programmed cell death characterized by iron-dependent phospholipid peroxidation, was first proposed in 2012[25]. It has been shown to participate in the onset and development of several degenerative retinal diseases, such as AMD[26], glaucoma[27], and diabetic retinopathy (DR)[28]. Recently, ferroptosis has also been demonstrated to be involved in oxidative stress-mediated RPE cell death[29–31]. However, the fundamental mechanism underlying blue light-induced RPE damage is still unclear.

In this study, through high-throughput sequencing and biochemical experiments, we revealed the novel finding that heme oxygenase-1 (HMOX1)-mediated ferroptosis was the dominant genetic pathway involved in blue light-induced damage to RPE cells. The involvement of ferroptosis in blue light-induced RPE dysfunction was proven for the first time. Furthermore, in ferroptotic RPE cells overexpressing HMOX1, both the knockdown of HMOX1 in vitro and the intraperitoneal injection of the HMOX1 inhibitor zinc protoporphyrin (ZnPP) in vivo were shown to successfully rescue damaged cells and degenerated retinas. Our findings provide a new perspective on blue light-induced RPE damage, and we believe that inhibiting HMOX1-mediated ferroptosis will be a promising targeted therapeutic strategy for blue light-related retinal damage in the future.

Results

Ferroptosis was shown to play an important role in blue light-induced damage to ARPE-19 cells

Based on previous reports, ARPE-19 cell has been widely validated and used as the typical cell lines to study RPE cell in vitro[32,33]. Therefore, to investigate the mechanism of blue light-induced RPE damage, blue light (BL) irradiation with an illumination intensity of 1500 lx and a peak wavelength of 421 nm was used to establish an ARPE-19 cell damage model. We compared blue light-induced cell damage with that induced by erastin-mediated cell ferroptosis as a positive control to determine whether the two types of damage had morphological and biochemical similarities. To assess the effects of blue light on RPE cell viability, live/dead staining and CCK-8 analysis were conducted. We observed that both blue light irradiation and erastin treatment for 24 h inhibited the survival of ARPE-19 cells (Fig. 1A–C). In addition, as shown in Supplementary Fig. 1, Edu staining assay revealed that the blue light suppressed the proliferation of ARPE-19 cells in vitro after treatment for 24 h. Moreover, pretreatment of ARPE-19 cells with the ferroptosis inhibitor DFO significantly reversed these effects, suggesting that ferroptosis may account for a significant proportion of blue light-induced damage to ARPE-19 cells (Fig. 1A-C). To further verify blue light-induced ferroptosis in ARPE-19 cells, the protein expression levels of the ferroptosis markers glutathione peroxidase 4 (GPX4) and acyl-CoA synthetase long-chain family member 4 (ACSL4) were measured[27]. Compared with the control group, the blue light-treated group presented lower expression levels of GPX4 and higher expression levels of ACSL4 (Fig. 1D, E). Consistent with the results of live/dead staining and CCK-8 analysis, these phenomena could be inhibited through pretreatment with DFO, further indicating that ferroptosis played an important role in blue light-induced damage to ARPE-19 cells.

Based on the above results, we performed RNA sequencing to better understand the types of cell death in ARPE-19 cells treated with blue light irradiation. Compared with those in the control group, in the blue light group, 114 genes were significantly upregulated, and 236 genes were significantly downregulated. These differentially expressed genes (DEGs) were further analysed through Kyoto Encyclopedia of Genes and Genomes (KEGG) enrichment analyses, which revealed that ferroptosis was the top pathway, above necrosis, apoptosis, autophagy, and other common cell death pathways, in blue light-induced damage to ARPE-19 cells (Fig. 1F).

Ferrous ion-catalyzed oxidation reaction was involved in blue light-induced ferroptosis in ARPE-19 cells

Since iron has been shown to play a catalytic role in ferroptosis[37], the intracellular ferrous ion level was assayed through FerroOrange staining. The results revealed excessive ferrous ions in both blue light-induced and erastin-treated ARPE-19 cells. However, preincubation with DFO significantly inhibited this effect (Fig. 2A,B). According to previous research, excess ferrous ion accumulation leads to the production of intracellular ROS and LOS, which causes increased harmful oxidative stress[25]. Thus, we subsequently conducted CM-H2DCFDA staining and C11-BODIPY staining to assess intracellular ROS and LOS levels, respectively. Consistent with the findings of previous studies, massive ROS and LOS generation was observed in the blue light and erastin groups, and pretreatment with DFO attenuated intracellular ROS and LOS accumulation, protecting ARPE-19 cells from oxidative damage (Fig. 2C–F). The above results showed that ferrous ion-catalysed oxidation was involved in blue light-induced ferroptosis in ARPE-19 cells, which was consistent with the findings of previous studies on ferroptosis induction[29,30].

HMOX1 upregulation contributed to ferroptosis in ARPE-19 cells

To further investigate the inherent mechanism of blue light-induced ferroptosis in ARPE-19 cells, a volcano plot was drawn to visualize the DEGs (Fig. 3A), and a heatmap was generated to visualize the ferroptosis-associated DEGs (Fig. 3B). HMOX1 was identified as the most upregulated gene in blue light-treated ARPE-19 cells, and the expression level of solute carrier family 7 member 11 (SLC7A11) was significantly elevated in the blue light group compared with the control group, which was consistent with the western-blot assay results (Fig. 3C,D). According to the literature, HMOX1 expression is regulated by several upstream transcription factors, including nuclear factor erythroid 2-related factor 2 (Nrf2), activator protein-1 (AP-1) and nuclear factor-kappa B (NF-κB)[38]. Among these genes, only Nrf2 was observed to have a significantly greater protein expression level, suggesting that the overexpression of HMOX1 is controlled by Nrf2 in blue light-treated ARPE-19 cells (Fig. 3E,F). Since previous research on ferroptotic tumour cells reported that the transcription of HMOX1 can be activated by the interaction of Nrf2 and SLC7A11[39].

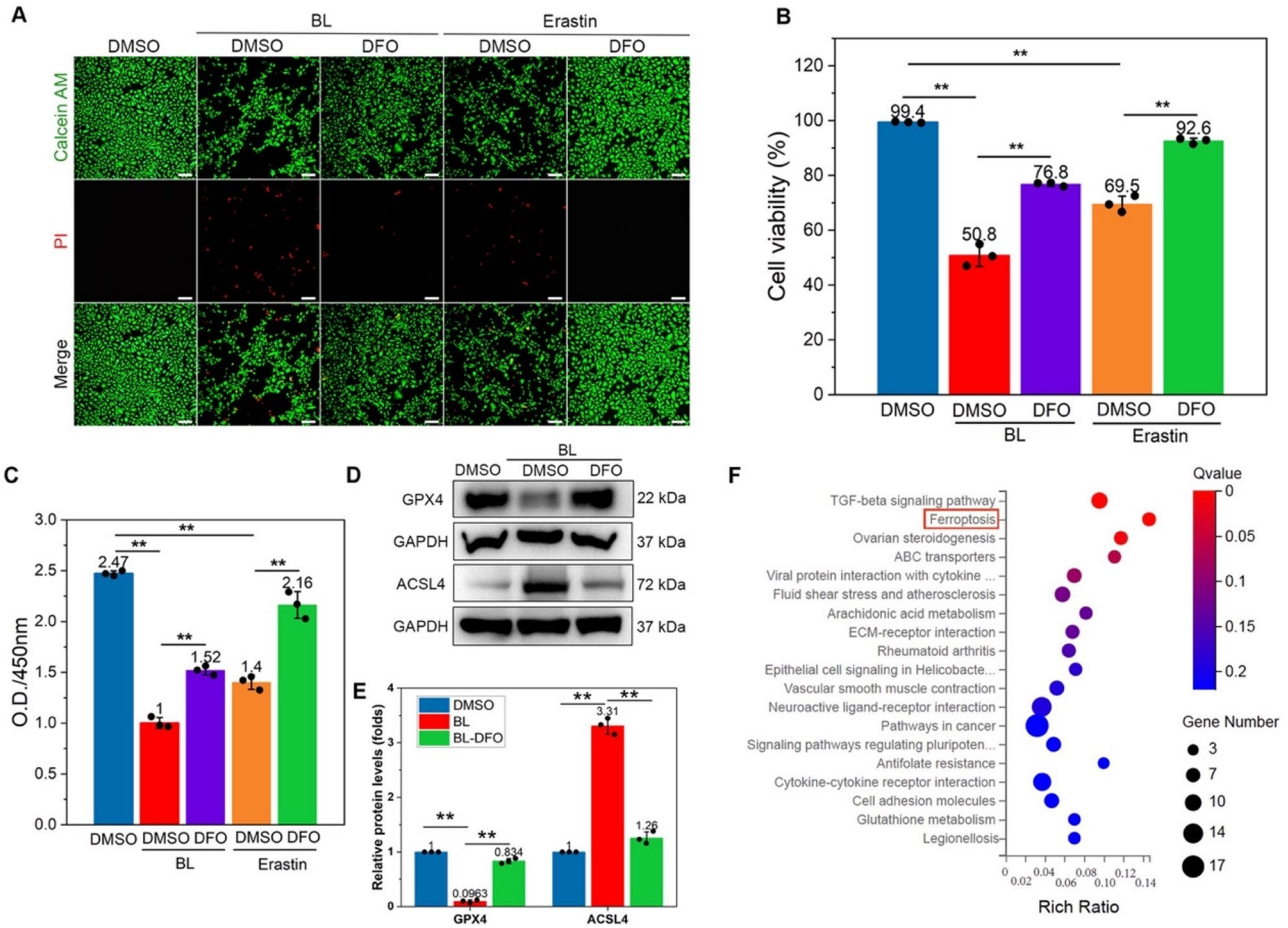

Fig. 1. Ferroptosis played an important role in blue light-induced damage of ARPE-19 cells. Blue light (BL) or ferroptosis inducer Erastin-treated ARPE-19 cells with or without ferroptosis inhibitor DFO exposure for 24 h, (**A**) cell survival and death were detected through live/dead staining. PI for dead cells and Calcein AM for live cells. Scale bar: 100 μm. DMSO treatment alone was used as a control. (**B**) Quantitative results of the cell viability for the statistical analysis by counting the live and dead cells using ImageJ software. $n = 3$, one-way ANOVA with Tukey's post hoc test, $^{**}p < 0.01$, data presented as mean ± SD. (**C**) CCK-8 analysis of cell viability by measuring the optical density of each well at 450 nm (O.D./450 nm) in each group. $n = 3$, one-way ANOVA with Tukey's post hoc test, $^{**}p < 0.01$, data presented as mean ± SD. (**D**) Protein expression level of the ferroptosis markers, GPX4 and ACSL4, and (**E**) their relative protein quantitation. $n = 3$, one-way ANOVA with Tukey's post hoc test, $^{**}p < 0.01$, data presented as mean ± SD. Original blots are presented in Supplementary Fig. 5. (**F**) KEGG enrichment analysis[34–36] identified the most significantly influenced pathways in response to blue light treatment. Copyright permission of KEGG pathway maps has been obtained.

Subsequently, western-blot assay was performed to further investigate whether the protein expression levels of HMOX1, Nrf2, and NF-κB could be affected by ferroptosis inhibitor DFO. As presented in Supplementary Fig. 2, DFO treatment showed no significant effects on the protein expression levels of HMOX1, Nrf2 and NF-κB in BL-treated ARPE-19 cells. We hypothesized that ferroptosis in ARPE-19 cells is the consequence of HMOX1 overexpression after exposure to blue light irradiation, and that DFO, as the downstream inhibitor of ferroptosis, may not affect the upstream protein expression of HMOX1, Nrf2 and NF-κB. These results emphasized the regulatory hierarchy of the activated Nrf2/HMOX1 signaling in BL-induced RPE ferroptosis.

Inhibition of HMOX1 upregulation protected ARPE-19 cells from ferroptosis in vitro

To investigate whether blocking the upregulation of HMOX1 protected ARPE-19 cells from blue light-induced ferroptosis, an siRNA (si-HMOX1) was used to inhibit the overexpression of HMOX1 in vitro[40], and a series of biological experiments were conducted subsequently. To evaluate the knockdown efficiency of HMOX1, western-blot assay was performed. Compared with untreated (CTRL) and si-NC transfected ARPE-19 cells, the HMOX1 protein expression in si-HMOX1 transfected ARPE-19 cells was significantly decreased, suggesting successful knockdown of HMOX1 in ARPE-19 cells (Supplementary Fig. 3A). As expected, the decrease in cell viability after exposure to blue light was reversed in si-HMOX1-transfected ARPE-19 cells (Fig. 4A,B), indicating that knockdown of HMOX1 could ameliorate blue light-induced damage to cells. For further observation of ferroptosis-specific biomarkers, FerroOrange staining, CM-H2DCFDA staining and C11-BODIPY staining

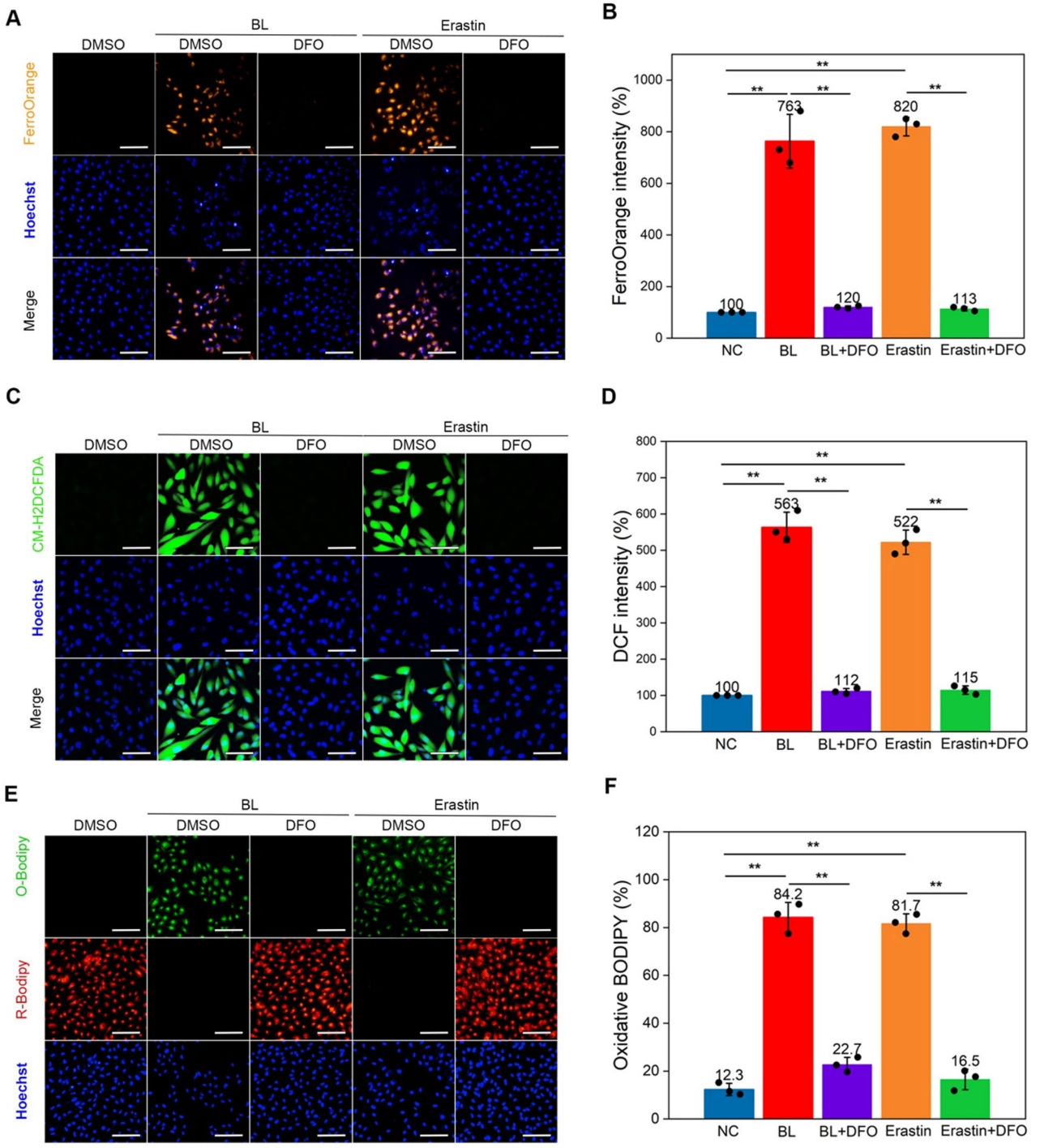

Fig. 2. Ferrous ion-catalysed oxidation reaction was involved in blue light-induced ferroptosis in ARPE-19 cells. (**A**) FerroOrange staining and (**B**) the relative fluorescence intensity of ferrous ions. Scale bar: 50 μm. $n = 3$, one-way ANOVA with Tukey's post hoc test, $^{**}p < 0.01$, data presented as mean ± SD. (**C**) CM-H2DCFDA staining and (**D**) the relative quantitation of intracellular ROS levels in ARPE-19 cells. Scale bar: 50 μm. $n = 3$, one-way ANOVA with Tukey's post hoc test, $^{**}p < 0.01$, data presented as mean ± SD. (**E**) BODIPY staining of LOS generation in ARPE-19 cells and (**F**) ratio of oxidative BODIPY. Scale bar: 50 μm. $n = 3$, one-way ANOVA with Tukey's post hoc test, $^{**}p < 0.01$, data presented as mean ± SD.

were conducted to investigate the impact of si-HMOX1 transfection on intracellular ferrous ion, ROS and LOS levels, respectively. We found that the accumulation of ferrous ions, ROS and LOS in ARPE-19 cells after blue light treatment was significantly inhibited by si-HMOX1 transfection (Fig. 4C–H), which indicated that the knockdown of HMOX1 protected ARPE-19 cells from ferrous ion-induced oxidative stress, preventing blue light-induced ferroptosis.

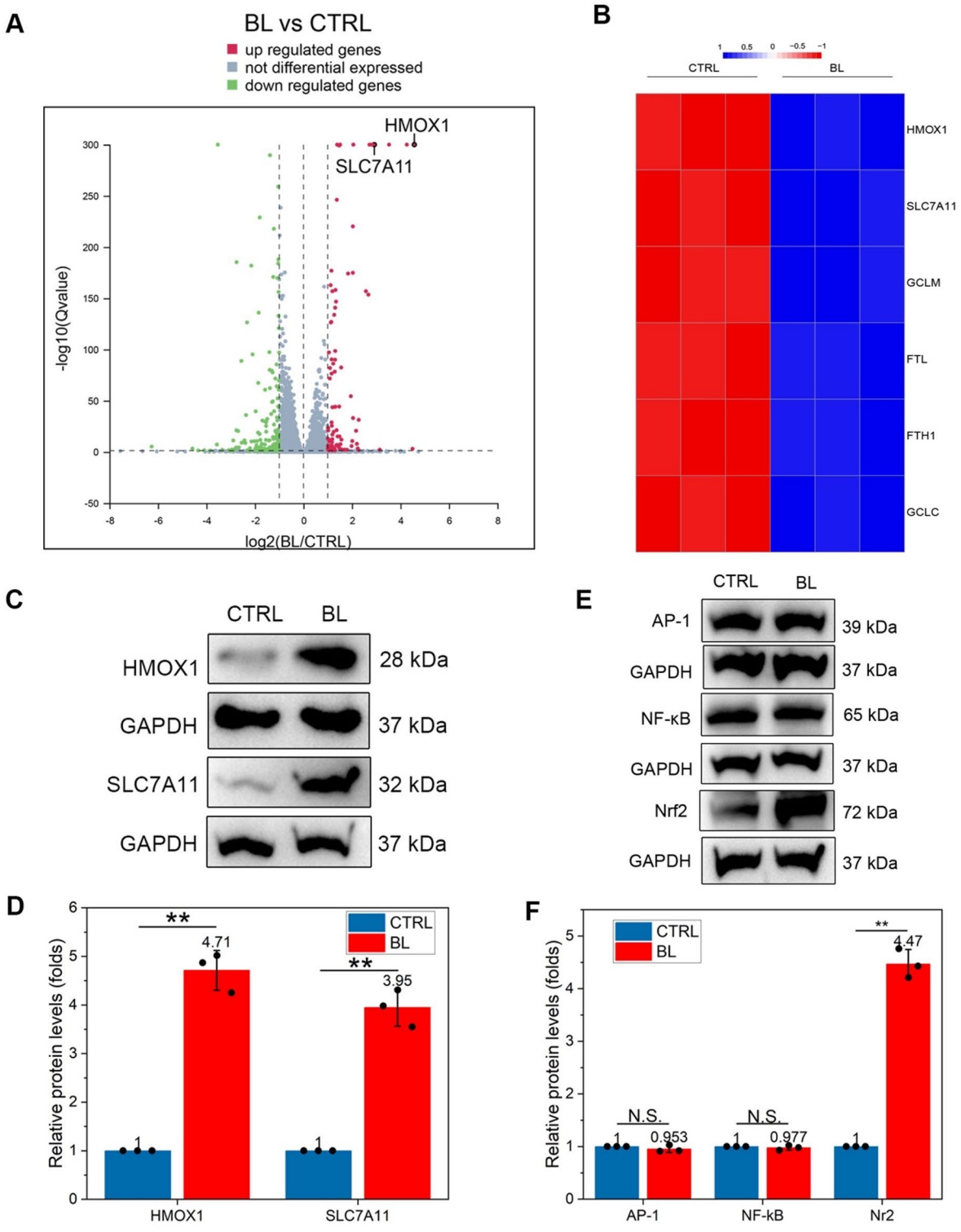

Fig. 3. HMOX1 upregulation contributed to ferroptosis in ARPE-19 cells. (**A**) The number of differentially expressed genes (upregulated in red and downregulated in green) was presented in a volcano plot from RNA-seq analysis. (**B**) Differentially expressed genes closely associated with ferroptosis in blue light-treated ARPE-19 cells were exhibited in heatmap. (**C**) Western-blot assay, and (**D**) relative protein quantitation of HMOX1 and SLC7A11 after treatment with blue light. $n = 3$, two-tailed Student's t-test, $^{**}p < 0.01$, data presented as mean ± SD. Original blots are presented in Supplementary Fig. 6. (**E**) Western-blot assay, and (**F**) relative protein quantitation of the upstream transcription factors, AP-1, NF-κB, and Nrf2. $n = 3$, two-tailed Student's t-test, $^{**}p < 0.01$, not significant (N.S.) > 0.05, data presented as mean ± SD. Original blots are presented in Supplementary Fig. 7.

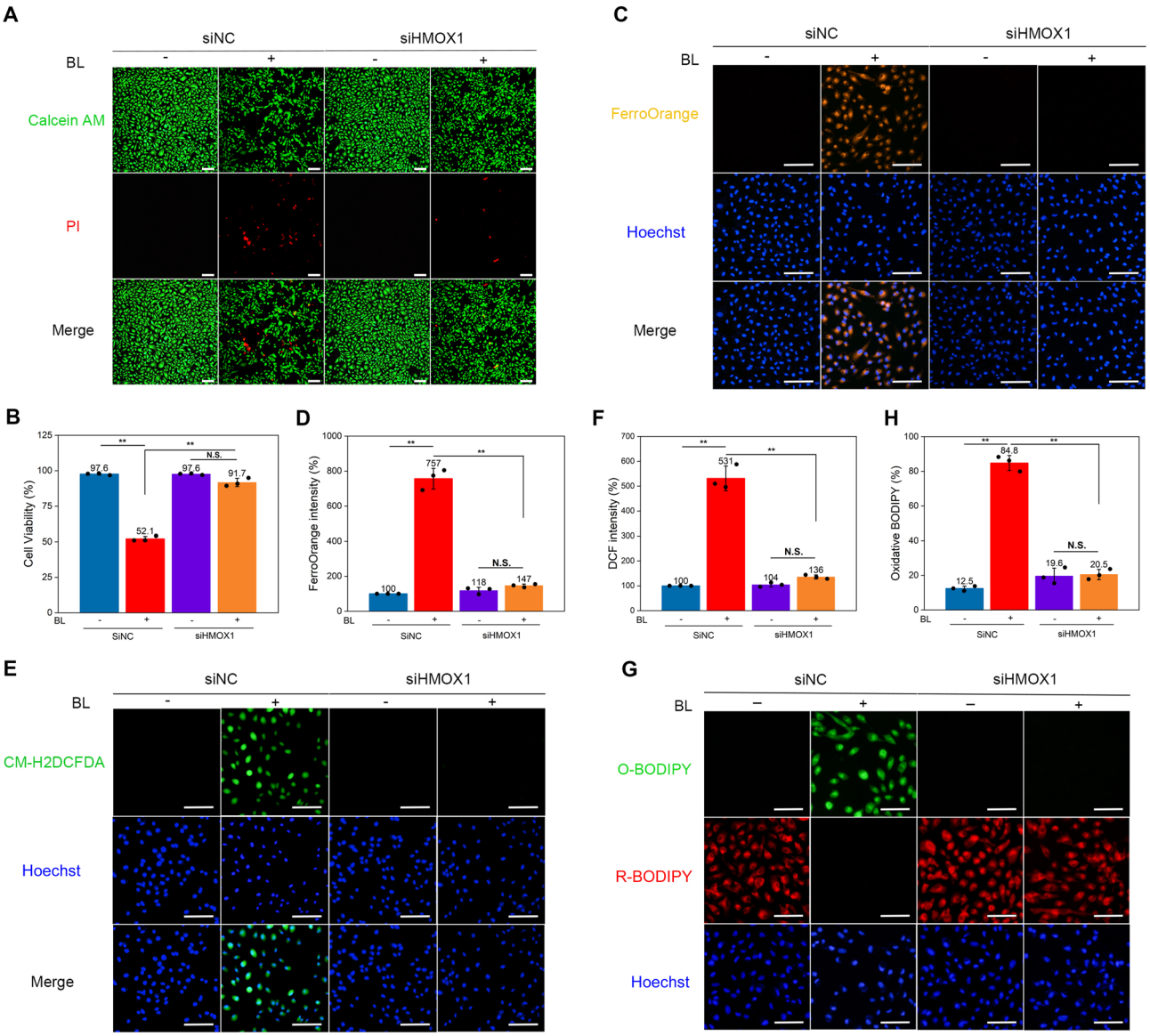

Fig. 4. Inhibition of HMOX1 upregulation protected ARPE-19 cells from ferroptosis in vitro. (**A**) Cell survival and death were detected through live/dead staining, and (**B**) quantitation of cell viability. Scale bar: 100 μm, $n = 3$, one-way ANOVA with Tukey's post hoc test, $^{**}p < 0.01$, not significant (N.S.) > 0.05, data presented as mean ± SD. (**C**) FerroOrange staining and (**D**) relative fluorescence intensity of ferrous ions. Scale bar: 50 μm. $n = 3$, one-way ANOVA with Tukey's post hoc test, $^{**}p < 0.01$, not significant (N.S.) > 0.05, data presented as mean ± SD. (**E**) CM-H2DCFDA staining and (**F**) relative quantitation of intracellular ROS level in ARPE-19 cells. Scale bar: 50 μm. $n = 3$, one-way ANOVA with Tukey's post hoc test, $^{**}p < 0.01$, not significant (N.S.) > 0.05, data presented as mean ± SD. (**G**) BODIPY staining of LOS generation in ARPE-19 cells and (**H**) ratio of oxidative BODIPY. Scale bar: 50 μm. $n = 3$, one-way ANOVA with Tukey's post hoc test, $^{**}p < 0.01$, not significant (N.S.) > 0.05, data presented as mean ± SD.

To further understand the role of HMOX1 in the BL-induced ferroptosis, the inhibitory effect of zinc protoporphyrin (ZnPP, a well-established selective HMOX1 inhibitor) was also investigated. As appeared in Supplementary Fig. 3B, HMOX1, which was obviously upregulated in BL-induced ARPE-19 cells, was successfully inhibited by ZnPP (10 μM) exposure. The reduction in HMOX1 protein levels by ZnPP also increased the cell viability, as indicated by a significant increase in Calcein AM-positive live cells, and inhibited ROS generation during the ferroptosis process by decreasing DCF fluorescence intensity (Supplementary Fig. 3C-F). In addition, blue light exposure decreased ZO-1 expression and disrupted cell morphology in ARPE-19 cells, which could be effectively rescued by ZnPP treatment (Supplementary Fig. 3G). These results suggested that the protective effect of HMOX1 inhibition on blue light-induced RPE ferroptosis is consistent with previous results that HMOX1 upregulation contributes to ferroptosis induced by oxidative stress[26].

Inhibition of HMOX1 upregulation prevented retinal damage caused by blue light exposure in vivo

To further verify whether inhibiting HMOX1 overexpression in vivo had the same effect as it had in vitro, ZnPP (50 mg/kg) was injected intraperitoneally once a week for 2 weeks. As presented in Supplementary Fig. 4A, blue light exposure for 2 weeks significantly upregulated HMOX1 expression in RPE layer in vivo, which is consistent with our previous research[26]. Fortunately, ZnPP treatment effectively decreased the HMOX1 expression level in blue light-treated mice. Additionally, H&E staining revealed retinal structural damage in the blue light group, especially in the disordered and reduced number of cells in the outer nuclear layer (ONL). Pigment disturbance and cell morphological changes in the RPE layer (marked by arrows) were observed, which were reversed in the ZnPP group (Fig. 5A). In addition, the protein expression level of the RPE tight junction biomarker ZO-1 was observed through immunofluorescence staining. We found that, after exposure to blue light, the expression level of ZO-1 was markedly lower than that in the control group, and pretreatment with ZnPP protected the tight junctions in the RPE (Fig. 5B,C). To understand the effects of ZnPP under BL conditions on RPE at the biomolecular level, we detected the RPE65 (the typical RPE cell biomarker) expression level by immunofluorescence staining. The results showed that blue light exposure decreased the RPE65 expression in RPE layer in vivo, which could be reversed upon ZnPP treatment (Supplementary Fig. 4B), suggesting the RPE protective effects by HMOX1 inhibition. As protection of visual function is the ultimate goal, a full-field electroretinogram (ERG) was performed to assess whether inhibition of HMOX1 could protect against visual functional damage caused by blue light. Rod photoreceptor responses to light stimulation under scotopic conditions were tested during the ERG experiment. The results revealed that blue light-treated mice presented a significant reduction in the ERG curve, indicating damage to visual function. However, ZnPP preadministration significantly improved retinal function, as indicated by a greater amplitude of both the a- and b-waves in the ERG graphs (Fig. 5D, E). To further investigation into the effects of blue light exposure with or without ZnPP treatment on photoreceptor cells, immunofluorescence staining of typical photoreceptor-involved biomarkers, Arrestin in mouse retina was conducted. Compared with PBS-treated mice, blue light-exposed retina exhibited the decreased fluorescence intensity of Arrestin, which was significantly reversed using ZnPP treatment (Fig. 5F). Taken together, these results suggested that inhibition of HMOX1 overexpression prevented retinal damage caused by blue light exposure in vivo, which might be a potential clinical treatment strategy for blue light-induced retinal damage.

Discussion

In the present study, the hypothesis that ferroptosis participates in blue light-induced RPE damage was proposed and verified by observations of decreased cell viability, downregulated GPX4 and upregulated ACSL4 protein expression levels and the accumulation of ferrous ions, ROS, and LOS in cells. DEGs between the blue light group and the control group were determined through high-throughput sequencing. Functional analyses identified ferroptosis as the main cell death pathway. Mechanistically, the overexpression of HMOX1 played a key role in blue light-induced ferroptosis in ARPE-19 cells, which may be associated with the Nrf2–SLC7A11–HMOX1 hierarchy. In addition, si-HMOX1 and ZnPP were used to inhibit the overexpression of HMOX1 in vitro and in vivo, respectively, resulting in the protection of ARPE-19 cells from ferroptosis and retinal damage after exposure to blue light. Collectively, these results suggested that HMOX1-mediated ferroptosis is the dominant mechanism of blue light-induced RPE damage.

Concerns about the potential harm of blue light to the visual system are continuously increasing. As the receiver of light signals, the retina plays a vital role in vision. Within the ten-layer structure of the retina, the RPE is an important constituent that maintains the normal physiological structure of the retina. However, blue light can lead to structural and functional damage to the RPE, resulting in visual dysfunction. Previously, our group investigated the underlying mechanism of blue light-induced damage to the normal RPE. We found that inflammation and angiogenesis are associated with blue light-induced damage to normal ARPE-19 cells. This study builds on our previous findings and presents more in-depth research on the mechanism of retinal damage caused by blue light irradiation. In addition, experiments have shown that the susceptibility of the retina to light injury is influenced by the circadian rhythm[41,42]. Exposure to blue light at night was shown to cause more severe damage to the retina of mice than exposure during the day, which might be associated with fluctuations in circulating corticosterone levels in mice[43,44]. Therefore, in this study, blue light was turned on between 8:00 am and 10:00 am, followed by 12 h of day–night circulation to avoid disruption of the internal biological clock.

Heme oxygenase is the enzyme that degrades endogenous iron protoporphyrin haem and catalyses the rate-limiting step of the reaction, resulting in the production of biliverdin, ferrous ions, and carbon monoxide, with biliverdin being further reduced to bilirubin[45]. Oxygenase has three active isoforms, namely, HMOX1, HMOX2, and HMOX3, with HMOX1 being an inducible isoform. The expression level of HMOX1 can be upregulated under various stress conditions, including UV irradiation, infection, exposure to heavy metals, and cytokines[46]. HMOX1 extensively participates in ROS homeostasis and iron detoxification and plays a dual role in ferroptosis. In 2015, Kwon et al. reported that HMOX1 accelerated Erastin-triggered ferroptosis[47]. Subsequently, Chang et al. reported that HMOX1 is a key mediator of BAY 11-7085-induced ferroptotic cell death, indicating that HMOX1 is a promising chemotherapeutic target for cancer treatment[39]. Additionally, particulate matter induces ferroptosis in microglia through excessive iron accumulation by activating Nrf2/HMOX1 pathway[48]. However, studies by Adedoyin et al. suggested that HMOX1 could attenuate ferroptosis in renal proximal tubule cells and protect against acute kidney injury[49]. One explanation for the ambivalent role of HMOX1 in ferroptosis is that its activation could lead to either beneficial or detrimental effects on cells, depending on the extent of HMOX1 upregulation[50]. To investigate the effect of HMOX1 levels on cell viability and ferrous ions, in our previous study, we treated the ARPE-19 cells with the HMOX1 inducer hemin at different concentrations. It has been found that high, but not low, concentrations of hemin caused a significant reduction of cell viability and an overload

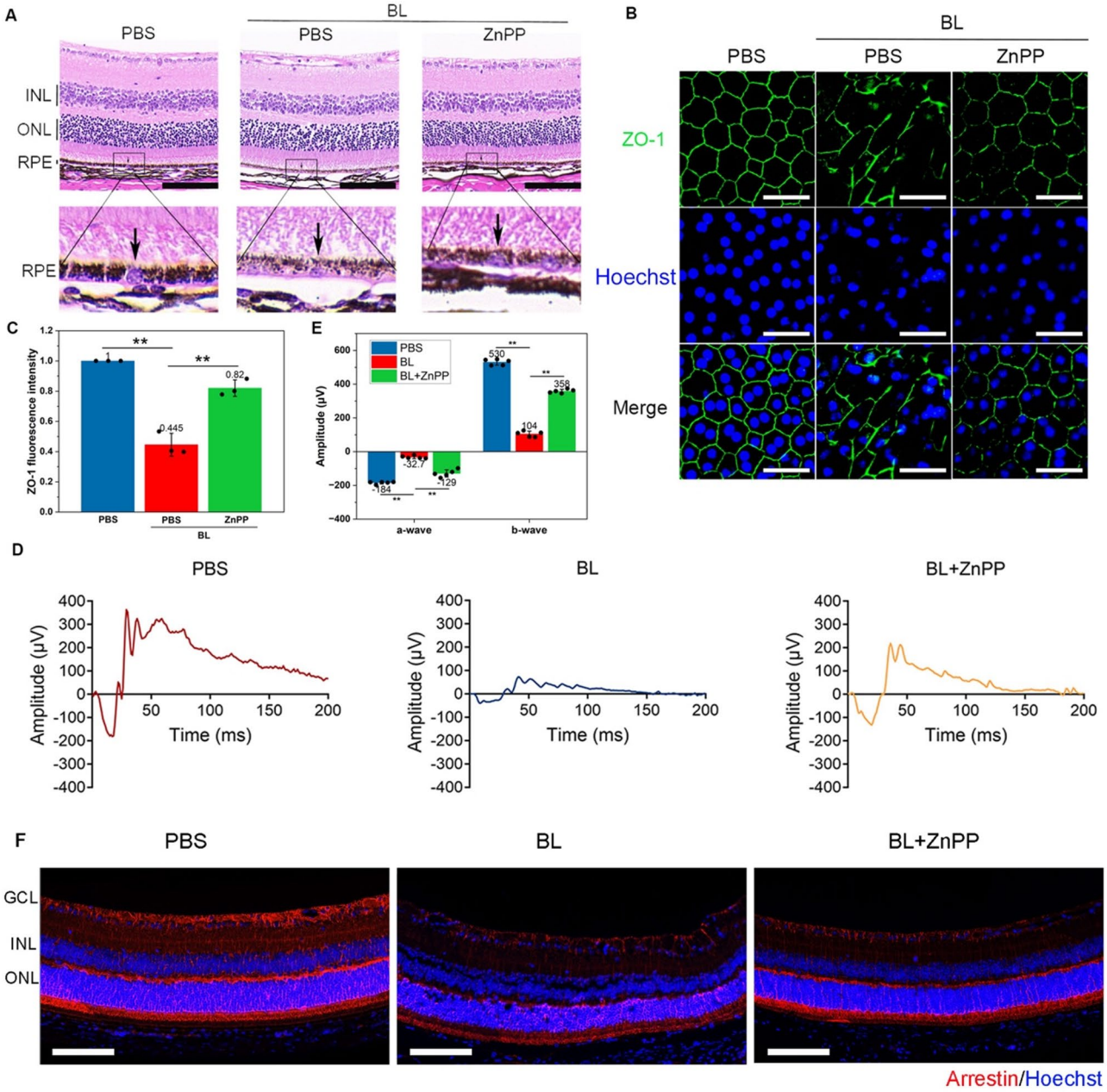

Fig. 5. Inhibition of HMOX1 upregulation prevented retinal damage caused by blue light exposure in vivo. (**A**) H&E staining showed pigmentation and morphological changes in the RPE pretreated with the HMOX1 inhibitor ZnPP, followed by blue light treatment. Scale bar: 25 μm. Black arrows: RPE cells. ONL: outer nuclear layer, INL: inner nuclear layer. (**B**) Immunofluorescent staining and (**C**) relative fluorescence intensity of RPE tight junction biomarker ZO-1. Scale bar: 25 μm. $n = 5$, one-way ANOVA with Tukey's post hoc test, $^{**}p < 0.01$, data presented as mean ± SD. (**D**) The visual functions of mice in the control, blue light and ZnPP groups were detected through ERG. (**E**) ERG a- and b-wave amplitude values were measured. $n = 5$, one-way ANOVA with Tukey's post hoc test, $^{**}p < 0.01$, data presented as mean ± SD. (**F**) After mice with different treatment for 14 days, immunofluorescence staining of typical photoreceptor biomarkers, Arrestin in mouse retina was performed. Scale bar: 100 μm. Hoechst (blue): nuclei. Arrestin: red. ONL: outer nuclear layer, INL: inner nuclear layer, GCL: ganglion cell layer.

of ferrous ions, suggesting that a substantial upregulation, but not a slight increase of HMOX1, exerts cytotoxic effects[26]. In this study, the results of RNA-seq and biological experiments revealed a strong upregulation of HMOX1, leading to the ferroptosis in ARPE-19 cells, which is consistent with the results of previous studies[51]. Therefore, HMOX1 may be a potential biomarker in some degenerative diseases with different extent of stimuli, such as oxidative stress. Based on HMOX1 level, either inhibition or upregulation of HMOX1 may serve as a potential therapeutic strategy.

In addition, to further evaluate the impact of HMOX1 on mice exposed to blue light, intraperitoneal injection of HMOX1 inhibitor ZnPP was performed. Fortunately, previous studies have validated the feasibility of intraperitoneal injection in mice with various retinal diseases[26,52,53]. For instance, intraperitoneal administration of propranolol in an oxygen-induced retinopathy mouse model significantly ameliorated retinopathy of prematurity by reducing the formation of abnormal retinal neovascularization, and decreased the leaking, tortuous, and abnormally expanding retinal blood vessels[52]. In addition, intraperitoneal injection of ilimaquinone effectively reduced laser-induced choroidal neovascularization in rabbits and mice[53]. These studies suggested that intraperitoneal injection in animals may be a feasible route for retinal therapy.

The literature shows that some enhancer sequences exist for the combination of redox-sensitive transcription factors, which act as upstream promoters of HMOX1, including Nrf2, AP-1, and NF-κB[38]. Nrf2 is the main transcriptional regulator of HMOX1 and anchors to the cytoplasm by forming a complex in the basal state. Some external stimuli cause Nrf2 to dissociate from the complex and translocate to the nucleus to exert its effects[54–57]. AP-1 is a redox-sensitive transcription factor that modulates gene expression when cells are exposed to oxidative stress[58]. Under fundamental conditions, NF-kB remains in an inactive form in the cytoplasm through sequestration of its inhibitory protein IkB. When a specific stimulus is present, IκB kinase is activated, leading to the phosphorylation and degradation of IκB, which ultimately results in the translocation of NF-κB subunits into the nucleus to regulate the transcription of the target gene. Nrf2 can interact with SLC7A11, leading to the activation of HMOX1, which ultimately causes ferroptosis in cancer cells[39], which is consistent with our results.

In summary, this study revealed the novel finding that ferroptosis plays an important role in blue light-induced damage to the RPE, which is predominantly regulated by HOMX1. Importantly, targeted inhibition of HOMX1 overexpression significantly suppressed blue light-induced RPE ferroptosis, providing a potential target for protection against retinal photodamage.

Materials and methods

Materials

Erastin, deferoxamine (DFO), ZnPP were purchased from Selleck Chemicals. Cell counting kit-8 (CCK-8) reagent, live/dead kit, and FerroOrange were purchased from Dojindo. CM-H2DCFDA and C11-BODIPY were obtained from Thermo Scientific. DMSO were obtained from Sigma-Aldrich. DMEM medium, penicillin/streptomycin, and fetal bovine serum (FBS) were bought from Gibico. Other chemicals were bought from New Cell & Molecular Biotech unless stated otherwise.

Cell culture and drug treatment

Human RPE (ARPE-19) cell line was purchased from the Cell Bank of the Chinese Academy of Sciences. Cells were cultured in DMEM medium (Gibco, USA) with 10% FBS (Gibco, USA) and 1% penicillin/streptomycin (Gibco, USA) at 37℃ with 5% CO_2 in incubator. During the in vitro experiments, the plating density of ARPE-19 cells was 8000 cells $well^{-1}$ in 96-well plates, 50,000 cells $well^{-1}$ in 24-well plates, and 200,000 cells $well^{-1}$ in 6-well plates. ARPE-19 cells were pretreated with DFO (dissolved in DMSO, 75 μM) for 30 min before exposed to blue light irradiation.

ZnPP (S7880; Selleck) was dissolved in 0.2 M NaOH, the pH adjusted to 7.4 with hydrochloric acid[59], and then diluted with saline to a concentration of 1 mg ml^{-1}. To evaluate the role of HMOX1 in vitro, ARPE-19 cells were pre-treated with ZnPP at a final concentration of 10 μM for 1 h prior to the blue light exposure.

Blue light irradiation parameter

The blue light LED lamp panel composed of 30 × 30 blue LED (1 W) array was bought from EVERFINE (China) with the main wavelength of 434.4 nm and peak wavelength of 421.2 nm. The illumination intensity was controlled to 1500 lx and the distance between illuminant and cells was 30 cm, which imitate the maximum illumination of electronic devices to human eyes in daily life. Besides, the influence of heat radiation output was ignorable. Cells in the treatment group were irradiated after DFO treatment for 30 min. ARPE-19 cells seeded on 6 or 24-well plates were exposed to blue light for 24 h.

CCK-8 assay and live/dead staining

CCK-8 assay and live/dead staining were applied to evaluate cell viability in ARPE-19 cells with or without the pretreatment of the inducer or inhibitor of ferroptosis after blue light exposure. Live/dead kit (PI for dead cells and Calcein AM for live cells) was used to stain the cells seeded in 24-well plates. After staining at 37℃ for 15 min, at least three random fields of photos were taken with fluorescence microscope (Nikon). Live and dead cells were counted using ImageJ software. Relative cell viability (%) was calculated as (number of Calcein AM-positive live cells /total cell number in the field) × 100%.

In CCK-8 assay, cells were seeded in 96-well plates and incubated with CCK-8 kit (Dojindo Molecular Technologies, Japan, 10μL $well^{-1}$) at 37℃ for 4 h. The EPOCH2 microplate reader (ELX800, BioTeK, USA) was used to measure the optical density of each well at 450 nm (O.D./450 nm). The cell viability was determined by calculating the values of O.D./450 nm in each group.

Edu staining assay

The Cell Light 5-ethynyl-20- deoxyuridine (Edu) Cell Proliferation Kit was bought from Guangzhou RiboBio, China. ARPE-19 cells were seeded in 24-well plates and incubated with Edu reagent at 37℃ for 2 h. After discarding the Edu medium mixture, 4% paraformaldehyde (PFA) fixed the samples for 20 min at 37 °C and then stained with an Apollo Dye Solution. Hoechst 33,342 was applied to stain the nucleic acids for another 20 min. A fluorescence microscope (Nikon, Japan) was employed to obtain the images.

Immunocytochemistry staining of ZO-1

ARPE-19 cells were seeded on sterile coverslips and embedded in 24-well plates. Cells after treatment were fixed with 4% PFA for 30 min and then were blocked with 10% goat serum in PBS. Protein expression level of ZO-1 in cells were measured by reacting with ZO-1 primary antibody (#33-9100, Invitrogen, 1:200). After that cells were reacted with secondary anti-mouse antibody-conjugated with Alexa Fluor® 594 (#A-11005, Invitrogen 1:800), and nucleus were stained with Hoechst (#BL1145B, Biosharp, 1:2000), fluorescence photos were imaged by fluorescence microscope.

Western-blot assay

ARPE-19 cells were suspended in protein lysis RIPA (New Cell & Molecular Biotech) consisting of proteinase and phosphatase inhibitors (New Cell & Molecular Biotech) to gain total proteins. Lysate proteins were further separated by SDS-PAGE electrophoresis (Bio-Rad, USA) and quickly transferred onto PVDF membranes (Millipore, USA). Membranes were blocked with 5% BSA for 1 h and then incubated overnight at 4℃ with the following antibodies: anti-GPX4 (#52455; CST; 1:1000), anti-ACSL4 (66617-1-lg; Proteintech; 1:1000), anti-Nrf2 ((#PA5-27882; Thermo Fisher, 1:500), anti-SLC7A11 (#12691; CST; 1:1000), anti-HMOX1 (#70081; CST; 1:1000), anti-GAPDH (#5174; CST; 1:2000), anti-NF-κB (#8242; CST; 1:1000), and anti-AP-1 (#9165; CST; 1:1000). After incubation, membranes were washed with TBST and then probed with secondary antibodies correspondingly (anti-mouse IgG #7076 or anti-rabbit IgG #7074; CST; 1:3000). Membranes were washed again with TBST and then RP-conjugated reagent by Tanon-5200 was used for protein chemical visualization.

Detection of intracellular ferrous ions and oxidative stress

FerroOrange (#F374; Dojindo), CM-H2DCFDA (#C6827, Invitrogen), and C11-BODIPY (#D3861, Invitrogen) were used for live cell fluorescent levels of total intracellular ferrous ions, reactive oxygen species (ROS), and lipid ROS (LOS), respectively. After specific treatment, ARPE-19 cells in 24-well plates were incubated with FerroOrange (5 μM), CM-H2DCFDA (10 μM), or C11-BODIPY (10 μM) probes in Hank's balanced salt solution (HBSS) for 30 min at 37 ℃, and then were washed three times with PBS. Fluorescence images were taken by a fluorescence microscope with the excitation wavelength of 488 nm. The fluorescence intensity of FerroOrange, DCF and oxidized/reduced BODIPY were calculated by ImageJ software. The percentages of ferrous ion and ROS levels were determined by quantitating and calculating the ratio of FerroOrange and DCF fluorescence intensities in treated groups to that in control groups, respectively. The percentage of LOS was calculated as (oxidized BODIPY fluorescence intensity /total BODIPY fluorescence intensity in the field) × 100% in each group.

siRNA transfection

For the knockdown of HMOX1, ARPE-19 cells were seeded in 6-well plates and transfected with siRNA after adherence, following the instruction of manufacturer (GenePharma). The sequence of siHMOX1 was UCUU GCACUUUGUUGCUGGTT (antisense5'-3'). Lipofectamine 3,000 transfection reagent (Invitrogen) was used for transient transfection. After 6 h, culture medium was refreshed and the transfected ARPE-19 cells were cultivated for 24 h in the incubator before further experiments.

Blue light damage animal model

In the study, male C57BL/6J mice (3-week-old) were purchased from Shanghai JiHui Laboratory Animal Care Co., Ltd. and housed in a standard laboratory environment. We confirm that all methods were carried out under the approval of the Institutional Animal Care Committee of the Ninth People's Hospital, Shanghai Jiao Tong University School of Medicine (Permission No. SH9H-2023-A827-1). In addition, we confirm that all methods are reported in accordance with ARRIVE guidelines, the GB/T 39,760 – 2021 Laboratory animal—Guidelines for euthanasia, and the regulations of the Institutional Animal Care Committee of the Ninth People's Hospital, Shanghai Jiao Tong University School of Medicine.

According to previous studies[53,60], intraperitoneal injection of ZnPP (50 mg kg^{-1} body weight) was performed to evaluate its impact on mice with blue light irradiation. All the C57BL/6J mice were divided into three groups randomly: (1) mice without any treatment (control group), (2) intraperitoneal injection of PBS 30 min before blue light irradiation (BL group); (3) intraperitoneal injection of ZnPP 30 min before blue light irradiation (BL + ZnPP group). Mice in group (2) and group (3) were exposed to blue light for 14 days keeping a 12 h blue light/dark cycle in transparent cages. The blue light LED lamp panel was placed about 30 cm above the mice to keep the illumination intensity to about 1500 lx in the cage. After illumination, the animal models were used for subsequent experiments.

Histological analyses

Histological analyses include hematoxylin and eosin (H&E) staining and immunofluorescence staining. At determined time, euthanasia was implemented by intraperitoneal injection of overdose sodium pentobarbital (150 mg kg^{-1} body weight)[61]. Then, the eyeballs of the mice were separated carefully with ophthalmic forceps and scissors with about 3 mm of the optic nerves retained. Then the eyes were immediately fixed in FAS eyeball fixative solution (Servicebio). After being embedded in paraffin and dehydrated with a series of ethanol solutions, the slices were cut to a thickness of 6 μm and stained with H&E. For immunofluorescence staining, slices were incubated with primary antibodies, including anti-ZO-1(#33-9100, Invitrogen, 1:200), anti-Arrestin (#85067-5-RR, Proteintech, 1:200), anti-HMOX1 (#86806; CST; 1:200), anti-RPE65 (#17939-1-AP; Proteintech, 1:200), overnight at 4℃, and then with alexa fluor 488/594-conjugated secondary anti-mouse antibodies for 1 h at room temperature. Nuclei were stained with Hoechst. A microscope was used to take images of H&E and immunofluorescence staining with white light or fluorescence.

Electroretinography (ERG)

Mice with dark adaption for 24 h were prepared beneath dim red light after being anesthetized with isoflurane (induction: 3% at 1.0 L min^{-1}; maintenance: 1.5% at 0.6 L min^{-1}), and pupils were dilated. The ground electrodes and the reference electrodes were attached to the tail and the forehead respectively. A pair of gold-ring electrodes were placed on the cornea of the left and right eyes. An Espion E3 instrument (Diagnosys, Boxborough, MA) was used to record the retinal response to light stimulation. A single flash stimulus of 10 cd*s m^{-2} was performed to elicit scotopic ERGs. After 5 min of light adaption, a flash with 30 cd*s m^{-2} intensity were used to induce Photopic ERGs. The a-wave amplitude equals the voltage value from the baseline to the lowest negative voltage, and the amplitude of b-wave measures the trough of the a-wave to the crest of the b-wave.

Statistical analysis

All the current statistics were shown as mean ± standard deviation (SD). Statistical analysis was carried out only for studies where each group size was at least $n = 3$, and these experiments are independent. One-way analysis of Variance (ANOVA) with Tukey's post hoc test for comparisons between multiple groups, and a two-tailed Student's t-test to compare two groups were performed for statistical analysis[62]. $P < 0.05$ was considered statistically significant.

Data availability

The direct link of the available RNA-sequencing data is https://www.ncbi.nlm.nih.gov/sra/PRJNA1251208.

Received: 2 October 2024; Accepted: 22 May 2025
Published online: 29 May 2025

References

1. Behar-Cohen, F. et al. Light-emitting diodes (LED) for domestic lighting: any risks for the eye? *Prog Retin Eye Res.* **30**(4), 239–257 (2011).
2. Sliney, D. H. What is light? The visible spectrum and beyond. *Eye (Lond).* **30**(2), 222–229 (2016).
3. Grimm, C. et al. Rhodopsin-mediated blue-light damage to the rat retina: effect of photoreversal of bleaching. *Invest. Ophthalmol. Vis. Sci.* **42**(2), 497–505 (2001).
4. Kuse, Y. et al. Damage of photoreceptor-derived cells in culture induced by light emitting diode-derived blue light. *Sci. Rep.* **4**, 5223 (2014).
5. Lougheed, T. Hidden blue hazard? LED lighting and retinal damage in rats. *Environ. Health Perspect.* **122**(3), A81 (2014).
6. Vicente-Tejedor, J. et al. Removal of the blue component of light significantly decreases retinal damage after high intensity exposure. *PLoS One.* **13**(3), e0194218 (2018).
7. Noell, W. K. et al. Retinal damage by light in rats. *Invest. Ophthalmol.* **5**(5), 450–473 (1966).
8. Biesemeier, A. et al. Iron accumulation in Bruch's membrane and melanosomes of donor eyes with age-related macular degeneration. *Exp. Eye Res.* **137**, 39–49 (2015).
9. Mitchell, P. et al. Age-related macular degeneration. *Lancet* **392**(10153), 1147–1159 (2018).
10. Sun, C., Zhou, J. & Meng, X. Primary cilia in retinal pigment epithelium development and diseases. *J. Cell. Mol. Med.* **25**(19), 9084–9088 (2021).
11. Shang, P. et al. Primary cell cultures from the mouse retinal pigment epithelium. *J. Vis. Exp.* **133** (2018).
12. Ramsay, E. et al. Role of retinal pigment epithelium permeability in drug transfer between posterior eye segment and systemic blood circulation. *Eur. J. Pharm. Biopharm.* **143**, 18–23 (2019).
13. Strauss, O. The retinal pigment epithelium in visual function. *Physiol. Rev.* **85**(3), 845–881 (2005).
14. Lehmann, G. L. et al. Plasma membrane protein Polarity and trafficking in RPE cells: past, present and future. *Exp. Eye Res.* **126**, 5–15 (2014).
15. Yang, S., Zhou, J. & Li, D. Functions and diseases of the retinal pigment epithelium. *Front. Pharmacol.* **12**, 727870 (2021).
16. Lin, C. H. et al. Low-Luminance blue Light-Enhanced phototoxicity in A2E-Laden RPE cell cultures and rats. *Int. J. Mol. Sci.* **20**(7) (2019).
17. Krigel, A. et al. Light-induced retinal damage using different light sources, protocols and rat strains reveals LED phototoxicity. *Neuroscience* **339**, 296–307 (2016).
18. Nakamura, M. et al. Exposure to excessive blue LED light damages retinal pigment epithelium and photoreceptors of pigmented mice. *Exp. Eye Res.* **177**, 1–11 (2018).
19. Ju, Y. et al. Protection against light-induced retinal degeneration via dual anti-inflammatory and anti-angiogenic functions of thrombospondin-1. *Br. J. Pharmacol.* **179**(9), 1938–1961 (2022).
20. Abdouh, M. et al. Filtering blue light mitigates the deleterious effects induced by the oxidative stress in human retinal pigment epithelial cells. *Exp. Eye Res.* **217**, 108978 (2022).
21. Nakamura, M. et al. The involvement of the oxidative stress in murine blue LED Light-Induced retinal damage model. *Biol. Pharm. Bull.* **40**(8), 1219–1225 (2017).
22. Sparrow, J. R. & Cai, B. Blue light-induced apoptosis of A2E-containing RPE: involvement of caspase-3 and protection by Bcl-2. *Invest. Ophthalmol. Vis. Sci.* **42**(6), 1356–1362 (2001).
23. Cheng, K. C. et al. The role of oxidative stress and autophagy in Blue-Light-Induced damage to the retinal pigment epithelium in zebrafish in vitro and in vivo. *Int. J. Mol. Sci.* **22**(3) (2021).
24. Hanus, J., Anderson, C. & Wang, S. RPE necroptosis in response to oxidative stress and in AMD. *Ageing Res. Rev.* **24**(Pt B), 286–298 (2015).
25. Dixon, S. J. et al. Ferroptosis: an iron-dependent form of nonapoptotic cell death. *Cell* **149**(5), 1060–1072 (2012).
26. Tang, Z. et al. HO-1-mediated ferroptosis as a target for protection against retinal pigment epithelium degeneration. *Redox Biol.* **43**, 101971 (2021).
27. Yao, F. et al. Pathologically high intraocular pressure disturbs normal iron homeostasis and leads to retinal ganglion cell ferroptosis in glaucoma. *Cell. Death Differ.* **30**(1), 69–81 (2023).
28. He, W. et al. Research progress on the mechanism of ferroptosis and its role in diabetic retinopathy. *Front. Endocrinol. (Lausanne).* **14**, 1155296 (2023).
29. Lee, J. J. et al. Lysosome-associated membrane protein-2 deficiency increases the risk of reactive oxygen species-induced ferroptosis in retinal pigment epithelial cells. *Biochem. Biophys. Res. Commun.* **521**(2), 414–419 (2020).
30. Shu, W. et al. Ferrous but not ferric iron sulfate kills photoreceptors and induces photoreceptor-dependent RPE autofluorescence. *Redox Biol.* **34**, 101469 (2020).

31. Sun, Y. et al. Glutathione depletion induces ferroptosis, autophagy, and premature cell senescence in retinal pigment epithelial cells. *Cell. Death Dis.* **9**(7), 753 (2018).
32. You, L. et al. Tyrosol protects RPE cells from H(2)O(2)-induced oxidative damage in vitro and in vivo through activation of the Nrf2/HO-1 pathway. *Eur. J. Pharmacol.* **991**, 177316 (2025).
33. Tang, Z. et al. Nanoprotection against retinal pigment epithelium degeneration via ferroptosis Inhibition. *Small Methods*. **5**(12), e2100848 (2021).
34. Kanehisa, M. et al. KEGG: biological systems database as a model of the real world. *Nucleic Acids Res.* **53**(D1), D672–D677 (2025).
35. Kanehisa, M. Toward Understanding the origin and evolution of cellular organisms. *Protein Sci.* **28**(11), 1947–1951 (2019).
36. Kanehisa, M. & Goto, S. KEGG: Kyoto encyclopedia of genes and genomes. *Nucleic Acids Res.* **28**(1), 27–30 (2000).
37. Ueda, K. et al. Iron promotes oxidative cell death caused by bisretinoids of retina. *Proc. Natl. Acad. Sci. U S A*. **115**(19), 4963–4968 (2018).
38. Medina, M. V. et al. Regulation of the expression of Heme Oxygenase-1: signal transduction, gene promoter activation, and beyond. *Antioxid. Redox Signal.* **32**(14), 1033–1044 (2020).
39. Chang, L. C. et al. Heme oxygenase-1 mediates BAY 11-7085 induced ferroptosis. *Cancer Lett.* **416**, 124–137 (2018).
40. Park, C. et al. Protective effect of phloroglucinol on oxidative stress-induced DNA damage and apoptosis through activation of the Nrf2/HO-1 signaling pathway in HaCaT human keratinocytes. *Mar. Drugs* **17**(4) (2019).
41. Organisciak, D. T. et al. Circadian-dependent retinal light damage in rats. *Invest. Ophthalmol. Vis. Sci.* **41**(12), 3694–3701 (2000).
42. Vaughan, D. K. et al. Evidence for a circadian rhythm of susceptibility to retinal light damage. *Photochem. Photobiol.* **75**(5), 547–553 (2002).
43. Fukuhara, C. et al. Gating of the cAMP signaling cascade and melatonin synthesis by the circadian clock in mammalian retina. *J. Neurosci.* **24**(8), 1803–1811 (2004).
44. Tosini, G., Ferguson, I. & Tsubota, K. Effects of blue light on the circadian system and eye physiology. *Mol. Vis.* **22**, 61–72 (2016).
45. Maines, M. D. The Heme Oxygenase system: a regulator of second messenger gases. *Annu. Rev. Pharmacol. Toxicol.* **37**, 517–554 (1997).
46. Ameriso, S. F. et al. Heme oxygenase-1 is expressed in carotid atherosclerotic plaques infected by Helicobacter pylori and is more prevalent in asymptomatic subjects. *Stroke* **36**(9), 1896–1900 (2005).
47. Kwon, M. Y. et al. Heme oxygenase-1 accelerates erastin-induced ferroptotic cell death. *Oncotarget* **6**(27), 24393–24403 (2015).
48. Wei, H. et al. PM(2.5)-induced ferroptosis by Nrf2/Hmox1 signaling pathway led to inflammation in microglia. *Environ. Pollut.* **352**, 124130 (2024).
49. Adedoyin, O. et al. Heme oxygenase-1 mitigates ferroptosis in renal proximal tubule cells. *Am. J. Physiol. Ren. Physiol.* **314**(5), F702–F714 (2018).
50. Gorrini, C., Harris, I. S. & Mak, T. W. Modulation of oxidative stress as an anticancer strategy. *Nat. Rev. Drug Discov.* **12**(12), 931–947 (2013).
51. Rossi, M. et al. Dual effect of Hemin on renal ischemia-reperfusion injury. *Biochem. Biophys. Res. Commun.* **503**(4), 2820–2825 (2018).
52. Su, S. et al. Propranolol ameliorates retinopathy of prematurity in mice by downregulating HIF-1α via the PI3K/Akt/ERK pathway. *Pediatr. Res.* **93**(5), 1250–1257 (2023).
53. Son, Y. et al. Ilimaquinone inhibits neovascular age-related macular degeneration through modulation of Wnt/β-catenin and p53 pathways. *Pharmacol. Res.* **161**, 105146 (2020).
54. Itoh, K. et al. Keap1 regulates both cytoplasmic-nuclear shuttling and degradation of Nrf2 in response to electrophiles. *Genes Cells.* **8**(4), 379–391 (2003).
55. Dinkova-Kostova, A. T. et al. Direct evidence that sulfhydryl groups of Keap1 are the sensors regulating induction of phase 2 enzymes that protect against carcinogens and oxidants. *Proc. Natl. Acad. Sci. U S A*. **99**(18), 11908–11913 (2002).
56. Baird, L. & Yamamoto, M. The molecular mechanisms regulating the KEAP1-NRF2 pathway. *Mol. Cell. Biol.*, **40**(13) (2020).
57. Yamamoto, M., Kensler, T. W. & Motohashi, H. The KEAP1-NRF2 system: a Thiol-Based Sensor-Effector apparatus for maintaining redox homeostasis. *Physiol. Rev.* **98**(3), 1169–1203 (2018).
58. Kim, H. et al. Redox regulation of lipopolysaccharide-mediated sulfiredoxin induction, which depends on both AP-1 and Nrf2. *J. Biol. Chem.* **285**(45), 34419–34428 (2010).
59. Jiang, X. X., Zhang, R. & Wang, H. S. Neferine mitigates angiotensin II-induced atrial fibrillation and fibrosis via upregulation of Nrf2/HO-1 and Inhibition of TGF-β/p-Smad2/3 pathways. *Aging (Albany NY)* **16**(10), 8630–8644 (2024).
60. Qi, X. et al. IL-37 inhibits inflammation of lacrimal gland in dry eye mice via the IL-37-PTEN-NFκB signaling pathway. *Ocul Immunol. Inflamm.* **32**(10), 2449–2458 (2024).
61. Laferriere, C. A., Leung, V. S. & Pang, D. S. Evaluating intrahepatic and intraperitoneal sodium pentobarbital or ethanol for mouse euthanasia. *J. Am. Assoc. Lab. Anim. Sci.* **59**(3), 264–268 (2020).
62. He, K. et al. Smoking aggravates neovascular age-related macular degeneration via Sema4D-PlexinB1 axis-mediated activation of pericytes. *Nat. Commun.* **16**(1), 2821 (2025).

Author contributions

C.J., Y.W., Z.T., P.G., and J.J. conceptualized the study. C.J., Y.W., and Z.T. designed the experiments. C.J., Y.W., Y. J., S.L. and X.C. performed the experiments. C.J., Y.W. and Z.T. wrote the manuscript. All authors have read and agreed to the published version of the manuscript.

Funding

This work was funded by National Key R&D program of China (2022YFA1105502, 2022YFA1105500), National Natural Science Foundation of China (82271131), and National Natural Science Foundation of China (32200618).

Declarations

Competing interests

The authors declare no competing interests.

Additional information

Supplementary Information The online version contains supplementary material available at https://doi.org/10.1038/s41598-025-03757-3.

Correspondence and requests for materials should be addressed to Z.T., P.G. or J.J.